

**MICROSTRUCTURAL AND MECHANICAL CHARACTERIZATION OF Ti6Al4V
CELLULAR STRUTS FABRICATED BY ELECTRON BEAM POWDER BED FUSION
ADDITIVE MANUFACTURING**

Cody Ewing*, Yan Wu†, Li Yang†

*Department of Mechanical Engineering, University of Louisville, Louisville, KY 40292

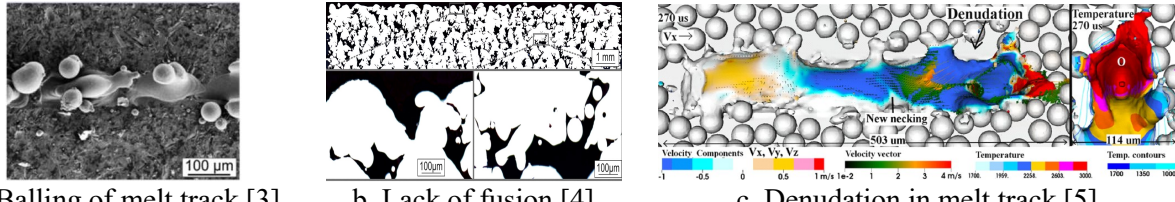
†Department of Industrial Engineering, University of Louisville, Louisville, KY 40292

Abstract

Despite the widespread use of the electron beam powder bed fusion (EB-PBF) additive manufacturing (AM) process in the fabrication of cellular structures, relatively little is known about the microstructural and mechanical properties of the individual cellular struts of different geometries fabricated by the EB-PBF. In this study, experimental investigation was carried out in the attempt to establish preliminary understanding of the material characteristics of the Ti6Al4V cellular struts using EB-PBF under various geometry design conditions (dimension and orientation angle). It was found that there exist significant geometry effects for the material characteristics of the Ti6Al4V cellular struts, which indicates that a non-uniform material model should be considered in the future design of these cellular structures.

Introduction

The electron beam based powder bed fusion (EB-PBF) additive manufacturing (AM) processes have been extensively utilized for the fabrication of cellular structures with highly fragmented cross sectional patterns due to their capability of realizing rapid beam deflection control, which enables more efficient cellular structure fabrication for EB-PBF compared to the laser based powder bed fusion (L-PBF) systems [1, 2]. On the other hand, it has also been widely recognized that the EB-PBF processes currently face various challenges. Some of these issues are associated with the intrinsic characteristics of the powder bed fusion (PBF) processes, which originates from the use of powder feedstock and the heat-based process principles. Due to the stochastic nature of the powder particle morphology and sizes, the PBF processes generally exhibit various process variability-related defects such as balling, lack of fusion and denudation, as shown in Fig.1 [3-5]. In addition, the thermal diffusion process that naturally occurs during the thermal cycles of the PBF processes also causes the sintering of powder particles on the exterior surfaces of the fabricated structures, which results in rough surface finish with the final parts [6-8]. For EB-PBF processes, due to the use of relatively coarse powder feedstock, larger beam diameter and higher preheating temperature, these intrinsic process variability issues are exacerbated compared to the L-PBF.



a. Balling of melt track [3] b. Lack of fusion [4]

c. Denudation in melt track [5]

Fig.1 Various process variability-related defects in PBF-AM

Literature has been shown that for the fabrication of bulk structures many of the defects generated by individual tracks can be alleviated or eliminated [9, 10]. However, in the fabrication of cellular structures, due to the small cross sectional areas and consequently fewer scan passes, much of the process variability-induced defects remain in the structures after the process. As a result, the cellular structures fabricated by PBF processes often exhibit more defects [11, 12]. Also, the small numbers of scanning tracks within the cross sections also implies that the fabrication of the PBF cellular structures is more sensitive to the selection of the scanning strategies and process parameters [11-14]. For example, the distributions of the porosities in the cellular struts fabricated via EB-PBF could exhibit concentric patterns that follow the boundaries between the hatch and contour regions [11]. Also, both the external geometry and the microstructure of the PBF cellular struts exhibit certain levels of defects even under optimized process parameters [11, 13, 15, 16]. Furthermore, it has also been demonstrated that the staircase effect resulted from the layerwise process becomes a significant quality factor for the PBF cellular structures [17, 18]. Such intrinsic property variability not only poses challenges to the performance design of the cellular structures but also their applicability in real-life applications, especially with load-critical structures where the defect-induced part failure can be of catastrophic consequence.

Relatively limited works have been carried out in the investigation of the unique microstructural and mechanical properties of the PBF cellular struts/materials and especially their dependencies on both the cross sectional geometries. In most of the previous literature the microstructural investigation focuses on the process setting (e.g. energy densities, beam energies), and the mechanical property evaluations were carried out at the cellular structure levels [11-16]. Such approach can become inefficient as the material properties of individual cellular struts are often coupled with the geometry effects, which could introduce infinite design variables into the analysis due through cellular geometry designs. In order to establish comprehensive understanding with the material characteristics of the PBF cellular structures, investigation that focuses on the individual strut level is needed. One earlier study along this direction has revealed that even for struts with relatively large cross sectional dimensions (1-2mm), the cellular material still exhibits significant process-geometry dependency [19]. It was shown that both the strut diameter and strut build orientation are significant factors for the mechanical properties of the fabricated cellular struts. In [19] the studies were carried out with the L-PBF process, whereas in many cases the EB-PBF is the preferred process choice for cellular structure fabrication due to its higher productivity as previously mentioned. Therefore in the current work an experimental study was carried out to characterize both the microstructure and the mechanical properties of cellular struts fabricated via EB-PBF to provide quantitative information into the process-geometry-property relationships of the Ti6Al4V EB-PBF cellular materials.

Experimental Procedures

The AM system and material used in this study are the Arcam S400 and Ti6Al4V-ELI (Arcam/AP&C). The powder feedstock was characterized by Microtrac S3000 particle size analyzer, which yield mean particle size $D_m=57.23\mu\text{m}$ with $D_{10}=48.68\mu\text{m}$, $D_{50}=64.23\mu\text{m}$ and $D_{90}=102.3\mu\text{m}$. The Arcam EB-PBF systems utilize preconfigured process setting specifically for the fabrication of cellular structures, which was used as the default process setting in this study. The decision of not adjusting the process setting was due to the facts that it was controlled by a large set of process variables that are highly interactive to each other and that the process utilizes in-situ variable-parameter control driven by internal algorithms that are not accessible to users. In addition, it should be noted that as the system was calibrated manually by the users prior to this study, the quality of the electron beam might not be as optimized compared to the systems that are maintained by the OEM service team.

Micro-tensile coupons as shown in Fig.1a were designed with varying cross sectional thickness $d=0.7\text{mm}$, 0.9mm , 1.1mm , 1.3mm and 1.5mm , and fixed gauge length $L=15\text{mm}$. The coupons were fabricated in the Arcam S400 systems with the longitudinal axis orienting at 15° , 45° and 90° in relation to the build plane. Fig.1b shows the example of samples oriented at 15° angle. All the micro-tensile coupon samples were placed on substrates (Fig.1b) that were also fabricated by the process in order to facilitate the consequent coupon separation process.



a. Micro-tensile coupon design

b. Coupon arrays at 15° orientation

Fig.1 Experimental sample designs

After fabrication, the samples were cut off from the substrates using a band saw. The cross sectional dimensions of each samples were measured using a digital optical microscope (Olympus MX51). For each sample, the measurements were taken at 6 different locations along the two sides of the samples as shown in Fig.1a. The approximate regions of the measurements are also shown in Fig.1a, although accurate control of measurement locations were not deemed necessary. For each region, The measurement of the cross sections followed the method described by Suard et al. [15] by taking both the inscribed diameter D_i and circumscribed diameter D_c as shown in Fig.2a. Fig.2b shows an example of the measurement results for a sample. In the attempt to evaluate the porosities of the samples, the other dimensions of the samples were also measured by using a caliper, and the weight of the samples were measured by a digital scale with resolution of 0.001g . The densities of each samples were calculated by dividing the weights by volumes, and the results were compared to the reference solid density of Ti6Al4V ($4.33\text{g}/\text{cm}^3$) to determine the porosities.

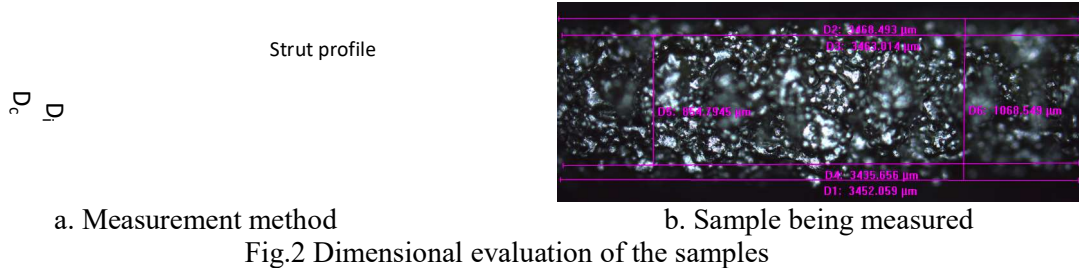


Fig.2 Dimensional evaluation of the samples

For the microhardness testing, one arbitrarily selected sample from each group were cut along the longitudinal xz or yz plane and mounted, and three random locations in the cross sections were selected from each samples for microhardness testing (Shimadzu HMV-G). The testing locations were selected in such a way that no obvious porosity was present in the testing area. For the micro-tensile testing, a custom testing fixture was made to accommodate the small sizes of the samples. As shown in Fig.3, a wrap-around testing fixture was designed and machined using 6061-T6 aluminum as material. During the testing, the two halves of the fixture were fixed on the tensile testing machine (Instron 5569A) using the default grips, and the samples were carefully inserted into one of the openings of the custom fixture. The spacing between the two halves of the custom fixture was then adjusted carefully to enable the other gripping end of the sample to be inserted into the other fixture opening. The sample was also aligned carefully to ensure that it was gripped vertically. A 5-10N pre-tension force was applied after the sample was fully inserted in order to retain the sample alignment. The tensile testing was carried out at 0.1mm/min constant displacement rate for all the samples.

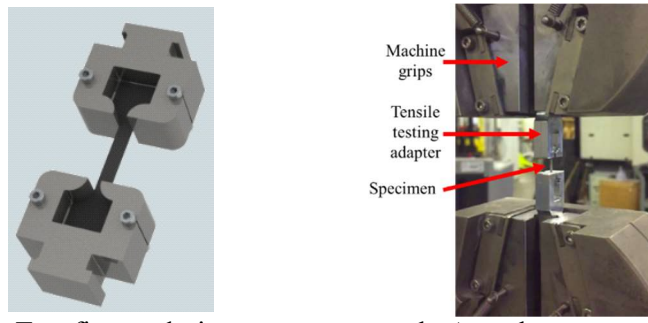


Fig.3 Micro-tensile testing fixture

Lastly, the microstructure of the samples was characterized using optical microscopy. The mounted samples for the micro-hardness testing were polished and etched before being characterized for microstructural phases as well as the dimensions of the grains. Previous studies have identified that the microstructure of the PB-EBF cellular struts exhibits columnar grain morphology oriented towards the build direction (i.e. Z-direction), with microstructural phases consist of both α -phase and α' -phase within the prior β grains [20-23]. In this study, the width of the columnar grains was measured from randomly selected grains within the micrographs for each types of sample.

Results and Discussions

Table 1 shows the dimensional and density measurement results for all the samples, and Fig.4 shows the relationships between the measurement results and the designed nominal dimensions

for all strut types. For all types of struts the designed dimensions fall between the maximum and minimum dimensions, i.e. between D_c and D_i . However, significant amount of dimensional variation between 300–500 μm was observed for all the struts, which accounts for as much as 50% of the nominal dimensions for small-size struts (0.7mm and 0.9mm). From previous studies it was suggested that the minimum inscribed diameters of the struts provide more close approximation for the mechanical property estimation of these struts [15, 24]. Based on such observations, it can be expected that all types of cellular struts fabricated by the EB-PBF process potentially exhibit reduced mechanical properties.

	Strut dim. D (mm)	D_c (mm)	D_i (mm)	D_c-D_i (mm)	$(D_c-D_i)/D$	Relative density
15	0.7	0.952±0.104	0.623±0.182	0.329±0.172	0.469	0.818±0.031
15	0.9	1.196±0.061	0.786±0.145	0.410±0.133	0.455	0.846±0.077
15	1.1	1.287±0.082	0.880±0.243	0.406±0.203	0.370	0.915±0.069
15	1.3	1.505±0.073	1.091±0.223	0.414±0.199	0.318	0.936±0.005
15	1.5	1.674±0.127	1.199±0.267	0.475±0.307	0.317	1.012±0.132
45	0.7	0.955±0.064	0.593±0.115	0.361±0.102	0.516	0.802±0.050
45	0.9	1.117±0.068	0.776±0.142	0.341±0.107	0.379	0.856±0.027
45	1.1	1.268±0.096	0.949±0.143	0.319±0.089	0.290	0.905±0.034
45	1.3	1.469±0.091	1.161±0.132	0.308±0.103	0.237	0.958±0.036
45	1.5	1.676±0.085	1.296±0.128	0.380±0.110	0.253	0.989±0.067
90	0.7	1.007±0.056	0.679±0.064	0.328±0.009	0.468	0.729±0.059
90	0.9	1.128±0.058	0.810±0.063	0.318±0.057	0.354	0.802±0.062
90	1.1	1.217±0.052	0.892±0.091	0.324±0.057	0.295	0.939±0.022
90	1.3	1.381±0.080	1.069±0.079	0.312±0.047	0.240	0.991±0.023
90	1.5	1.548±0.050	1.225±0.087	0.321±0.079	0.214	1.045±0.029

Table 1 Dimensional and density measurement results for different types of struts

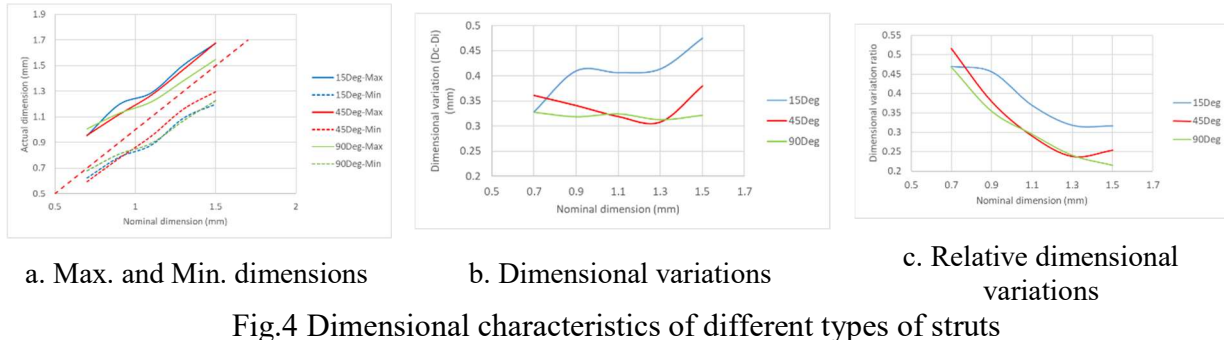


Fig.4 Dimensional characteristics of different types of struts

Also, from the results the struts fabricated at 15° orientation angle appear to exhibit the highest dimensional variability, whereas the 90° strut samples exhibit relatively consistent dimensional variability of around 320 μm . It is also noted that the 15° struts also exhibit largest variability of dimensional variations among multiple samples (Table 1), which clearly suggest that the dimensional quality of the low-angle struts is significantly compromised. This might be attributed to the oblique cross sectional areas of these struts that increases the tendency of defect generation when using the default network scanning strategy. On the other hand, the relative dimensional variation, which is defined as the ratio between the actual dimensional variation and the nominal dimension, steadily reduces as the nominal strut dimension increases.

The porosity measurement results show that in general there exist some porosities within the fabricated thin struts. There exist multiple measurement values that were larger than 1 that were obviously inaccurate, and this could be largely attributed by the use of overall dimensions for the estimation of the volumes of the parts, which could introduce some errors into the results. Regardless, the results still show that there exists clear trends between the geometrical type of the struts and their porosities. As shown in Fig.5, with increasing nominal strut dimensions the relative densities of the struts also increases. This agrees with the intuition that with smaller strut dimensions the EB-PBF process is more prone to generate internal defects to the structures. Also, it was observed that the 90° struts exhibit the highest relative density sensitivity relative to the nominal strut sizes. With small nominal strut size designs, the 90° orientation tends to result in the highest amount of internal porosities with the fabricated struts, which might be attributed to the small effective cross sectional areas at such orientation.

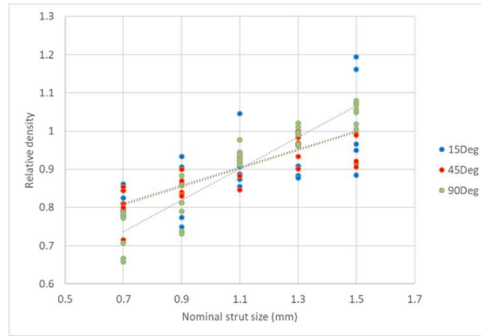


Fig.5 Relative density versus strut sizes and orientation angles

The microhardness and tensile strength of different types of struts are listed in Table 2, and the relationships between the mechanical properties and nominal strut sizes are shown in Fig.6. The microhardness of different types of struts exhibit relatively consistent hardness values of VHN350-380, which is slightly higher than the typical hardness from commercial Ti6Al4V materials [25-27], which might be contributed by the presence of the α' phase resulted from enhanced rapid cooling process. The tensile strength of different types of struts exhibit large differences as well as variabilities. While orientation angle appears to play less consistent role, the 15° struts exhibit significantly lower tensile strength of around 350-500MPa compared to the other two orientation types. The 45° struts exhibit slightly higher overall tensile strength as well as smaller strength variations across the entire dimensional ranges investigated, which might be due to their combinational characteristics of relatively small dimensional variability and porosities. Such observation is further illustrated in Fig.7, in which the tensile strength of all different types of struts are mapped against the relative densities of the struts. It is also noted that the lack of correlations between the relative density and the tensile strength of the struts is likely a result of the inaccurate calculation of relative density values, which does not adequately account for the large dimensional variability of the struts as previously discussed. With small-size struts, the strength variability of both 15° and 90° struts can exceed 250MPa, which would cause significant challenges with the reliable use of cellular structures with such strut dimensions. In addition, the tensile strength for all the struts are significantly lower than the solid Ti6Al4V fabricated via the same process previously reported [28], which again is attributed to the extensive presence of defects.

Strut angle (Deg)	Strut dim. D (mm)	Microhardness (VHN)	Max. strength (MPa)
15	0.7	382.62±18.36	464.04±267.94
15	0.9	370.75±10.35	479.84±149.91
15	1.1	357.41±7.24	354.99±51.50
15	1.3	376.30±28.57	341.14±82.21
15	1.5	368.75±27.72	483.60±108.69
45	0.7	386.97±8.58	852.80±91.00
45	0.9	376.89±15.04	689.35±38.36
45	1.1	376.18±12.49	649.54±143.95
45	1.3	367.88±11.29	767.74±26.48
45	1.5	355.13±17.35	748.70±54.01
90	0.7	376.08±8.61	752.80±262.04
90	0.9	376.89±10.36	740.76±119.33
90	1.1	367.72±3.38	540.14±35.28
90	1.3	377.05±15.07	550.16±11.25
90	1.5	379.52±18.75	640.56±24.50

Table 2 Microhardness and tensile strength of different types of struts

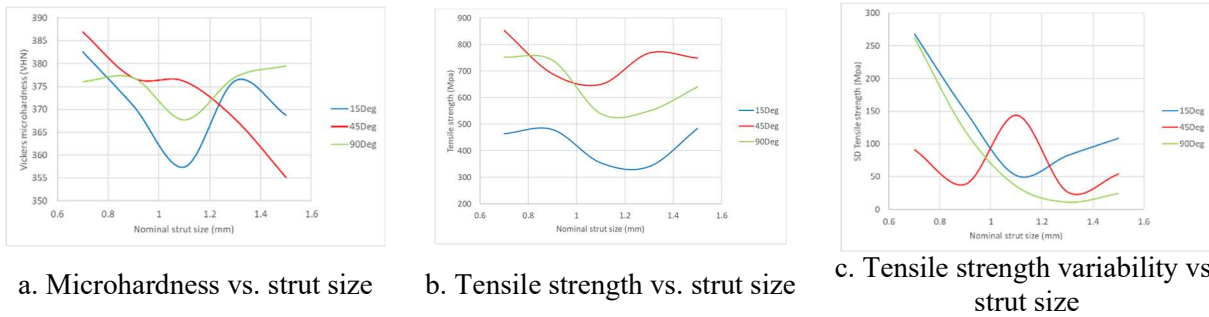


Fig.6 Mechanical properties of different types of struts

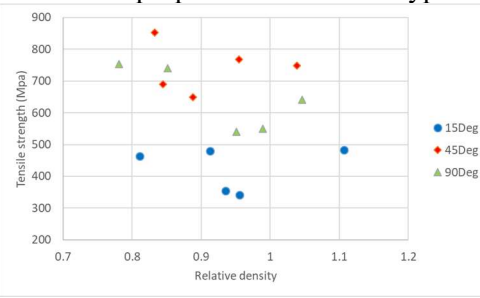
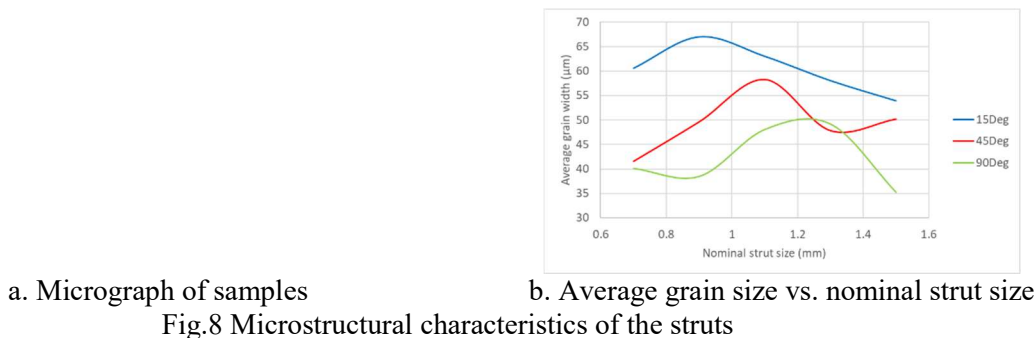


Fig.7 Tensile strength vs. relative density for different types of struts

Lastly, the microstructural characteristics of the strut samples are shown in Fig.8. The microstructure of the fabricated struts exhibit predominantly α phase with small amount of α' presence found in sporadic regions. The average grain width of the struts show clear dependency on the strut orientation, which 15° struts exhibit largest average grain width and 90° struts exhibit smallest average grain width. As the width of the grains is closely associated with the cooling rate during the solidification process, it was speculated that the smallest effective cross sectional areas of the 90° samples contributed to the more enhanced cooling rates during the fabrication process, which results in more refined microstructure. Despite the microstructural refinement, it was believed that both the in-process annealing effect and the presence of more extensive internal defects contributed to the lack of mechanical property enhancement from the 90° struts.



a. Micrograph of samples

b. Average grain size vs. nominal strut size

Fig.8 Microstructural characteristics of the struts

Conclusions

In this work the potential effects of geometry parameters including cross sectional dimensions and orientations on the quality characteristics of the Ti6Al4V cellular struts fabricated via EB-PBF process were evaluated. Despite the potential energy beam quality issues, the results revealed that there exist significant correlations between the geometry parameters and various geometrical, microstructural and mechanical characteristics of the cellular struts. For struts with very small cross sectional dimensions (<0.9mm), both the dimensional and mechanical qualities are significantly affected, which could impose significant challenges to the high-fidelity designs of these structures. This challenge could be further aggravated considering the fact that many lightweight cellular structures require the use of small-dimension struts. The low-orientation angle struts (i.e. struts that are more aligned towards the build substrate plane) exhibit larger dimensional variability and lowest overall mechanical strength, whereas the high-orientation angle struts (i.e. struts that are more aligned towards the build direction) exhibit highest dimensional qualities. On the other hand, likely due to the small effective cross sectional area, the high-orientation angle struts exhibit higher tendency of internal defect (porosity) generation with the increase of nominal strut dimensions, which negatively impacts their mechanical strength. With the anticipation that such process will be increasingly utilized for the design optimization with lightweight structures, the adequate understanding of the quality characteristics of the cellular struts becomes critical. The current study only provides a preliminary view into the problem, and more studies are needed towards the establishment of a comprehensive material database for PBF-AM cellular structures.

Acknowledgement

The authors are grateful of the support from Rapid Prototyping Center (RPC) at University of Louisville.

References

- [1] J. Parthasarathy, B. Starly, S. Raman, A. Christensen. Mechanical evaluation of porous titanium (Ti6Al4V) structures with electron beam melting (EBM). *Journal of the Mechanical Behavior of Biomedical Materials*. 3(2010): 249-259.
- [2] L. E. Murr, S. M. Gaytan, D. A. Ramirez, E. Martinez, J. Hernandez, K. N. Amato, P. W. Shindo, F. R. Medina, R. B. Wicker. Metal fabrication by additive manufacturing using laser and electron beam melting technologies. *Journal of Materials Science and Technology*. 28(2012), 1: 1-14.

- [3] L. Lober, F. P. Schimansky, U. Kuhn, F. Pyczak, J. Eckert. Selective laser melting of a beta-solidifying TNM-B1 titanium aluminide alloy. *Journal of Materials Processing Technology*. 214(2014): 1852-1860.
- [4] A. Bauereiss, T. Scharowsky, C. Korner. Defect generation and propagation mechanism during additive manufacturing by selective beam melting. *Journal of Materials Processing Technology*. 214(2014): 2522-2528.
- [5] S. A. Khairallah, A. T. Anderson, A. Rubenchik, W. E. King. Laser powder-bed fusion additive manufacturing: physics of complex melt flow formation mechanisms of pores, spatter, and denudation zones. *Acta Materialia*. 108(2016): 36-45.
- [6] J. C. Fox, S. P. Moylan, B. M. Lane. Effect of process parameters on the surface roughness of overhanging structures in laser powder bed fusion additive manufacturing. *Procedia CIRP*. 45(2016): 131-134.
- [7] I. Yadroitsev, I. Smurov. Surface morphology in selective laser melting of metal powders. *Physics Procedia*. 12(2011): 264-270.
- [8] G. Strano, L. Hao, R. M. Everson, K. E. Evans. Surface roughness analysis, modelling and prediction in selective laser melting. *Journal of Materials Processing Technology*. 213(2013): 589-597.
- [9] C. Korner, A. Bauereiss, E. Attar. Fundamental consolidation mechanisms during selective beam melting of powders. *Modelling and Simulation in Materials Science and Engineering*. 21(2013): 085011.
- [10] W. King, A. T. Anderson, R. M. Ferencz, N. E. Hodge, C. Kamath, S. A. Khairallah. Overview of modelling and simulation of metal powder bed fusion process at Lawrence Livermore National Laboratory. *Materials Science and Technology*. 31(2015), 8: 957-968.
- [11] E. Hernandez-Nava, C. J. Smith, F. Derguti, S. Tammas-Williams, F. Leonard, P. J. Withers, I. Todd, R. Goodall. The effect of defects on the mechanical response of Ti-6Al-4V cubic lattice structures fabricated by electron beam melting. *Acta Materialia*. 108(2016): 279-292.
- [12] S. Eosoly, G. Ryder, T. Tansey, L. Looney. Accuracy and mechanical properties of open-cell microstructures fabricated by selective laser sintering. *Proceedings of the Solid Freeform Fabrication (SFF) Symposium*, Austin, TX, 2007.
- [13] C. Qiu, S. Yue, N. J. E. Adkins, M. Ward, H. Hassanin, P. D. Lee, P. J. Withers, M. M. Attallah. Influence of processing conditions on strut structure and compressive properties of cellular lattice structures fabricated by selective laser melting. *Materials Science and Engineering A*. 628(2015): 188-197.
- [14] C. Yan, L. Hao, A. Hussein, P. Young, J. Huang, W. Zhu. Microstructure and mechanical properties of aluminium alloy cellular lattice structures manufactured by direct metal laser sintering. *Materials Science and Engineering A*. 628(2015): 238-246.
- [15] M. Suard, P. Lhuissier, R. Dendievel, J.-J. Blandin, F. VIgnat, F. Villeneuve. Towards stiffness prediction of cellular structures made by electron beam melting (EBM). *Powder Metallurgy*. 57(2014), 3: 190-196.
- [16] G. Campoli, M. S. Borleffs, S. Amin Yavari, R. Wauthle, H. Weinans, A. A. Zadpoor. Mechanical properties of open-cell metallic biomaterials manufactured using additive manufacturing. *Materials and Design*. 49(2013): 957-965.

- [17] C. Yan, L. Hao, A. Hussein, P. Young, D. Raymont. Advanced lightweight 316L stainless steel cellular lattice structures fabricated via selective laser melting. *Materials and Designs*. 55(2014): 533-541.
- [18] O. Cansizoglu, O. Harrysson, D. Cormier, H. West, T. Mahale. Properties of Ti-6Al-4V non-stochastic lattice structures fabricated via electron beam melting. *Materials Science and Engineering A*. 492(2008): 468-474.
- [19] G. Reinhart, S. Teufelhart, F. Riss. Investigation of the geometry-dependent anisotropic material behavior of filigree struts in ALM-produced lattice structures. *Physics Procedia*. 39(2012): 471-479.
- [20] N. W. Hrabe, P. Heinl, B. Flinn, C. Korner, R. K. Bordia. Compression-compression fatigue of selective electron beam melted cellular titanium (Ti-6Al-4V). *Journal of Biomedical Materials Research, Part B: Applied Materials*. 99(2011), 2: 313-320.
- [21] X.Y. Cheng, S. J. Li, L. E. Murr, Z. B. Zhang, Y. L. Hao, R. Yang, F. Medina, R. B. Wicker. Compression deformation behavior of Ti-6Al-4V alloy with cellular structures fabricated by electron beam melting. *Journal of the Mechanical Behavior of Biomedical Materials*. 16(2012): 153-162.
- [22] Y. Zhai, H. Galarraga, D. A. Lados. Microstructure evolution, tensile properties, and fatigue damage mechanisms in Ti-6Al-4V alloys fabricated by two additive manufacturing techniques. *Procedia Engineering*. 114(2015): 658-666.
- [23] S. J. Li, L. E. Murr, X. Y. Cheng, Z. B. Zhang, Y. L. Hao, R. Yang, F. Medina, R. B. Wicker. Compression fatigue behavior of Ti-6Al-4V mesh arrays fabricated by electron beam melting. *Acta Materialia*. 60(2012): 793-802.
- [24] L. Yang, O. Harrysson, H. West, D. Cormier. Compressive properties of Ti-6Al-4V auxetic mesh structures made by electron beam melting. *Acta Materialia*. 60(2012): 3370-3379.
- [25] ASM Matweb Ti6Al4V Grade 5 Spec Sheet:
<http://asm.matweb.com/search/SpecificMaterial.asp?bassnum=mtp641>.
- [26] S. S. da Rocha, G. L. Adabo, G. E. P. Hernriques, M. A. A. Nobilo. Vickers hardness of cast commercially pure titanium and Ti-6Al-4V alloy submitted to heat treatments. *Brazilian Dental Journal*. 17(2006), 2: 126-129.
- [27] X. Ma, F. Li, J. Cao, J. Li, H. Chen, C. Zhao. Vickers microhardness and microstructure relationship of Ti-6Al-4V alloy under cyclic forward-reverse torsion and monotonic torsion loading. *Materials and Design*. 114(2017): 271-281.
- [28] K. Rafi, H. Karthik N. V., T. L. Starr, B. E. Stucker. Mechanical property evaluation of Ti-6Al-4V parts made using electron beam melting. *Proceedings of the Solid Freeform Fabrication Symposium*, Austin, TX, 2012.